Conditional Instability and Shear for Six Hurricanes over the Atlantic Ocean

PAUL B. BOGNER AND GARY M. BARNES

Department of Meteorology, University of Hawaii, Honolulu, Hawaii

JAMES L. FRANKLIN*

NOAA/AOML/Hurricane Research Division, Miami, Florida

(Manuscript received 14 June 1999, in final form 1 November 1999)

ABSTRACT

One hundred and thirty Omega dropwindsondes deployed within 500-km radius of the eye of six North Atlantic hurricanes are used to determine the magnitudes and trends in convective available potential energy, and 10–1500-m and 0–6-km shear of the horizontal wind as a function of radius, quadrant, and hurricane intensity.

The moist convective instability found at large radii (400–500 km) decreases to near neutral stability by 75 km from the eyewall. Vertical shears increase as radius decreases, but maximum shear values are only one-half of those found over land. Scatter for both the conditional instability and the shear is influenced chiefly by hurricane intensity, but proximity to reflectivity features does modulate the pattern. The ratio of the conditional instability to the shear (bulk Richardson number) indicates that supercell formation is favored within 250 km of the circulation center, but helicity values are below the threshold to support strong waterspouts.

The difference between these oceanic observations and those made over land by other researchers is evidence for significant modification of the vertical profile of the horizontal wind in a hurricane at landfall.

1. Introduction

What is the vertical kinematic and thermodynamic structure of a hurricane over the sea? Establishing this base state is the first step in determining how the vertical gradients evolve during landfall. The Omega dropwindsonde (ODW) provides the raw data required for estimates of conditional instability, and vertical wind shear within the hurricane circulation. These parameters are vital for forecasts of supercell formation and attendant severe weather within the hurricane circulation.

Dropwindsondes have three advantages over aircraft flight-level data: first, one need not assume stationarity over a few hours to determine the vertical gradients of any variable; second, measurements are obtained in the lower mixed and surface layers where aircraft cannot safely fly; and third the ODW provides increased vertical resolution.

a. Prior work

Launched from either continent or island, the rawinsonde has served as the basis for numerous studies of hurricane vertical structure since the 1940s. These include Jordan and Jordan (1954), Jordan (1958), Sheets (1969), Novlan and Gray (1974), Frank (1977), McBride and Zehr (1981) and McCaul (1991). Only Novlan and Gray (1974) and McCaul (1991) quantified values of vertical wind shear, and only after landfall. Jordan and Jordan (1954) studied 300 Atlantic and Caribbean rawinsonde launches which occurred within 6° latitude of the hurricane center from 1946 to 1952. Temperature analyses revealed a warm core above 400 mb of 2°–3°C. This would point to a general decrease in the conditional instability near the eye as the lower levels remained virtually unchanged. However, the exact amount of change in the conditional instability could not be quantified because they had no reliable moisture sensor.

Jordan (1958) established a mean nocturnal sounding (to avoid insolation problems with the sensors) for the hurricane season in the Carribean using ascents from 1946 to 1955 from Miami, San Juan, and Swan Island. This average hurricane season sounding contains modest convective available potential energy (CAPE) of 1350 J kg^{-1} and is characterized by a relatively moist mixed layer and drying above 850 mb.

Sheets (1969) expanded upon the Jordan and Jordan (1954) mean hurricane soundings by concentrating on

* Current affiliation: National Hurricane Center, NWS, NOAA, Miami, Florida.

Corresponding author address: G. M. Barnes, Dept. of Meteorology, University of Hawaii, 2525 Correa Road, Honolulu, HI 96822. E-mail: garyb@soest.hawaii.edu

the region within 185 km of the eye. He composited a total of 92 Atlantic and Caribbean rawinsonde launches from 1956 to 1967 and found that temperatures near the surface decreased (~1.3°C) with decreasing surface pressures while the upper levels warm (~5°C at 250 mb) making the profile increasingly moist adiabatic. The result was a decrease in CAPE as the eye is approached with the mean hurricane profile containing only 680 J kg^{-1}.

Using a network of 30 island stations in the northwest Pacific, Frank (1977) looked at 18 000 rawinsonde launches within 15° of the center of 278 typhoons and tropical storms to determine the structure beyond 75 km of the eye. Small decreases in near-surface temperature and a larger warming at upper levels point to a reduction in the conditional instability toward the center.

The discussion of the vertical shear of the horizontal wind first became an issue in the mid-1960s as observations of tornadoes during hurricane landfall increased. Studies of hurricanes that produced tornadoes (e.g., Pearson and Sadowski 1965; Hill et al. 1966; Orton 1970; Gentry 1983) increasingly identified the importance of the strong vertical shear present in the lowest 1500–2000 m. However, these studies did not address storms that failed to spawn tornadoes. It was not until Novlan and Gray (1974) that a composite analysis of tornadic and nontornadic hurricanes was completed.

McCaul (1991) stratified 1300 rawinsonde observations by radial distance, quadrant, and proximity to tornado locations in order to calculate values of CAPE, bulk Richardson number, bulk Richardson number shear (0–6-km vertical shear), cell-relative total helicity, and streamwise vorticity. We shall compare our findings to both Novlan and Gray (1974) and McCaul (1991) in section 4.

These previous studies provide a description of the vertical structure after the hurricane is over land. Soundings from larger, more mountainous islands are also likely to obscure the vertical structure of a hurricane over the sea. The ODW can provide observations in the hurricane that are uncompromised by any landmass.

b. Goals

We will employ the ODWs to examine the vertical thermodynamic and kinematic structures within 500 km of the circulation center for six Atlantic hurricanes. We seek a benchmark for the conditions over the ocean that serve as the initial condition for the changes that occur at landfall. Specific questions are as follows:

1) How does the conditional instability vary as a function of radial distance from the center and as a function of quadrant?
2) Does the vertical shear vary as a function of radial distance and quadrant?
3) Does proximity of the sounding to rainbands or the eyewall affect the kinematic and thermodynamic structure?
4) How does helicity vary as a function of radius?
5) Is there a region within 500 km of the center of the hurricane that is favorable for supercell formation?
6) Is the hurricane circulation over the ocean capable of producing supercells that are responsible for much of the severe local weather witnessed during and after landfall?

We will compare our results with those studies that used rawinsondes to determine the vertical structures over land. In particular, we will make direct references to the work by Sheets (1969), Novlan and Gray (1974), Frank (1977), and McCaul (1991). The comparison with these works will provide insight as to how the hurricane evolves at landfall.

2. Data quality control and analysis scheme

a. Instrument description

The ODW is jettisoned from the National Oceanic and Atmospheric Administration (NOAA) WP-3D and falls at ~7–8 m s^{-1} at higher altitudes and ~5 m s^{-1} in the lowest 100–200 mb. While descending, it transmits measurements of the air temperature, relative humidity, and pressure once a second. Wind measurements are made every 10 s by the receiving and retransmission of Omega navigational signals. Nominal accuracies for the individual ODW sensors are estimated by Govind (1975) and are summarized in Table 1. According to Franklin (1987), the wind speed and pressure accuracies given in the table are attained only through careful postprocessing of the raw data.

b. Instrument problems

The ODW postprocessing procedures and common error corrections are described by Franklin (1987) and Bogner (1997). We will describe only those errors and corrective procedures that impact this study.

After launch, a comparison of aircraft and initial ODW measurements reveals that the ODW's thermistor and hygristor require some time to adjust to the atmospheric conditions, on the order of 5 s for the thermistor and 30 s for the hygristor. Therefore, aircraft observations of temperature and humidity are used for the initial values. Upon splashdown, careful comparisons of ODW splash pressures with other ODWs, surface synoptic analyses if the sonde was dropped far from the hurricane

TABLE 1. The ODW sensors and associated accuracies.

Sensor type	Variable sampled	Accuracy	Resolution
Thermistor	Temperature	±0.5°C	0.1°C
Hygristor	Relative humidity	±5%	1%
Aneroid cell	Pressure	±2 mb	0.2 mb
Omega receiver	Wind speed	1–2 m s^{-1}	0.1 m s^{-1}

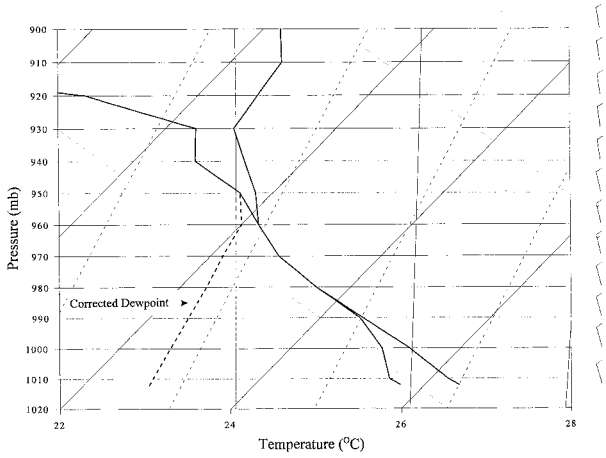

FIG. 1. Skew *T*–log*p* plot of ODW 3476 dropped in Gustav at a radius of 325 km. The bold solid lines show temperature and dewpoint, and the bold dashed line is the corrected dewpoint. Pressure in mb is shown by the thin horizontal lines, temperature lines are the thin solid lines that run from lower left to upper right, adiabats are light dotted lines running from lower right to upper left, mixing ratio lines are dashed, and the moist adiabats are vertical solid lines. Wind barbs are shown at right and follow standard notation. Mixing ratio lines are plotted every 2 g kg^{-1} starting with 22 g kg^{-1}.

center, and, when available, nearby buoys are used to identify errors due to pressure drift. These errors are corrected by hydrostatically computing the surface pressures using the ODW thermodynamic data and flight-level data.

Many of the problems that afflict the ODW can be attributed to liquid water. Two of the most frequent difficulties are thermistor shorting and wet-bulbing. When the thermistor shorts, temperature readings spike upward until the water evaporates away. These episodes are corrected by linear interpolation between the first and last good values, but if the spike lasts for longer than 100 mb, the data are lost.

Wet-bulbing occurs when an ODW drops out of a cloud into a region of much drier air. The evaporation of water on the thermistor cools the air surrounding the sensor resulting in a temperature estimate below the true air temperature. Instances of wet-bulbing are detected after plotting the data onto a skew *T*–log*p* diagram and are indicated by the occurrence of an inversion followed by a superadiabatic layer. In these soundings, the problem affects a thin layer that is corrected by linear interpolation. This problem is rare at convective cloud base (400–800 m) since air in the subcloud layer is usually very humid, which limits the rate of cooling.

Often the hygristor fails to dry out after passage through even thin cloud (Fig. 1). In these instances, the only possible correction to be made to the specific humidity profile is within the mixed layer where saturated conditions frequently were observed in conjunction with a dry-adiabatic temperature profile. Using a plot of potential temperature (θ), the height of the mixed layer is found by locating the point at which θ deviates from being constant (fully mixed). After locating the mixed layer height, we assume that the lifted condensation level (LCL) is 10 mb above the mixed layer top, the average depth of the transition layer, in accordance with our uncompromised soundings. Other studies of the tropical planetary boundary layer (e.g., Malkus 1958; NCAR 1977) demonstrate that the LCL is 5–15 mb above the top of the mixed layer. Upon plotting the LCL and the parcel θ on a thermodynamic diagram, the mean mixing ratio of the parcel is easily determined by tracing a mixing ratio line through the LCL (Fig. 1). We have tested our method for correcting soundings with complete moisture data from uncompromised ODWs and have found the resulting differences in the parcel mixing ratio not to show any bias and the estimates are within 0.5 g kg^{-1} of the actual parcel mixing ratio values. Any one sounding might suffer an error of this magnitude, but we will be interpreting soundings as a group and looking at the trends they might show as a function of radial distance. An erroneous sounding may increase the scatter, but will not mask significant trends.

c. Postprocessing

The 1-Hz data undergo a filtering process to reduce both the data volume and any short period fluctuations not previously removed. A 20-s (~10 mb) symmetric filter is used on the pressure, temperature, and humidity data. The symmetric filter runs with a maximum of 20 points spaced evenly around the central point or altitude to be determined. However, the filter remains symmetric even at altitudes that lie within 10 points of the surface or the last observation. In general, the total length of the filter is equal to the lesser of 20 points or one plus twice the actual number of points between the center point and the endpoint. This means that the first and last points are unfiltered and represent the initial aircraft reading and the last ODW reading before splashdown.

Franklin and Julian (1985) and Franklin (1987) describe how the winds are derived from the processing of the Omega navigation signals. Measurements of the signal phase are made every 10 s by eight worldwide Omega transmitters. The Omega signals from each of the stations are examined for signal quality and typically three to four are selected for the wind calculations. However, as many as seven stations may be used by the wind finding programs. Franklin and Julian (1985) state the addition of a fifth Omega station usually improves the wind measurements by 15%. Omega measurements are smoothed using a 3–4 min (~90 mb) filter. As a result of the large amount of filtering, the first and last 40 mb of the wind data are eliminated. The missing data just below aircraft level are filled in by linear interpolation between the aircraft and first ODW measurement. Within 40 mb of the sea surface we develop wind estimates based on the work of Powell (1980), who compared six different methods of estimating the 10-m winds from flight level. All the methods produce similar results and

fell within 10% of the buoy observations that serve as the baseline. Following Powell (1980), we have elected to assume that the speed at 10 m is 0.8 that found at 500 m. This 10-m wind will be used for shear calculations; we will discuss the uncertainty of the shear when we present those results. In the majority of cases, the available portion of the horizontal wind profile from the ODW yields a slope, which when continued to the surface, compares favorably to the formulated estimate of the surface wind speed.

The last of the sounding adjustments is to add a representative sounding top to turn the partial sounding (levels below 400 mb) into a complete sounding in order to make comparisons to prior analyses (Novlan and Gray 1974; McCaul 1991). The sounding tops were obtained from the Jordan and Jordan (1954) and Sheets (1969) composites. Sheets divides soundings (all within 185 km of the eye) into five categories based on decreasing pressures; whereas, Jordan and Jordan divides their soundings into five categories by distance from the hurricane circulation center (1°–6° of latitude). Both the Sheets and Jordan and Jordan sounding tops are added to all of the profiles according to the ODWs surface pressure and radial distance.

A comparison of CAPE values resulting from the addition of both the soundings tops reveals that the largest differences between the two occurred within 175 km of the eye and beyond 250 km. Between 175 and 250 km, CAPEs differ by only ± 25 J kg^{-1} due to a similar thermal structure within the sounding profiles. However, when contrasting the innermost and outermost profiles from each study, large differences arise that affect the CAPE distribution. Jordan and Jordan's innermost sounding is 2°C cooler than Sheets's at all levels above 700 mb, increasing CAPE by $\sim$200 J kg^{-1} nearer to the eyewall. The outermost sounding from Jordan and Jordan is also found to be cooler by 1°C, equivalent to an addition of $\sim$200 J kg^{-1} at 500-km radius.

The methodology employed in attaching a sounding top is to use the Jordan and Jordan soundings for all ODWs outside of 200 km as the temperatures and tropopause height are not heavily influenced by the warm core. Since Sheets's soundings were designed to describe the warm core structure, they are not considered representative of the outer hurricane environment but are used on all ODWs inside of 200 km. The actual attachment of the sounding top to the ODW data was completed by shifting the whole upper sounding profile to warmer or cooler values until it is aligned with the ODW profile. In other words, we accept the slope and tropopause height from either Sheets or Jordan and Jordan and do not allow any discontinuity in temperature at the attachment point. For 71% of the cases requiring shifting, the temperature of the attached sounding and the ODW profile differed by $\leq$1°C, 21% between 1.1° and 2°C and only 8% differed by greater than 2.1°C with the maximum being 4.2°C.

d. Sampled storms

The dataset consists of 130 ODWs deployed within 500 km of six Atlantic hurricanes sampled during the 1989, 1990, and 1995 seasons. The six hurricanes and their minimum sea level pressure at the time of sampling are Dean (979 mb), Gabrielle (927–941 mb), Hugo (918–938 mb), Gustav (959–978 mb), Iris (977 mb), and Luis (942 mb).

ODW locations with respect to the storm center are determined by two methods. The first requires the Tropical Prediction Center best track positions for each of the six hurricanes. The 6-h positions are accompanied by the minimum surface pressures and the maximum wind speeds. From this best track data, positions are determined for every half hour by linear interpolation to estimate the distance of the ODW launch to the storm center. In the second method we use lower fuselage radar scans to determine the distance from the reflectivity center of the hurricane. Differences in ODW locations obtained using these two methods were small ($\sim$10 km) and had their largest variations when drops occurred midway between the 6-h best track storm positions. The final position was therefore based on the linear interpolation of track. All the storms were sampled more than 500 km from the North American continent.

e. Stratifications and biases

During the sampling none of the hurricanes was strengthening or weakening more than a few millibars. Although the sondes are all launched during the afternoon and evening hours, the diurnal variations in temperature over the ocean ($\sim$1°C) are small enough as to not introduce any major biases (Frank 1977).

The ODW launches are initially stratified (Fig. 2) by quadrants relative to storm motion and radial distance from the storm center at increasing increments: 0–25 (eye), 25–50, 50–150, 150–300, and 300–500 km. Notice that the region 25–50 km from the center does not have a single ODW launch. This region includes the eyewall where the strong updrafts and high liquid water contents would seriously compromise the ODW. The distribution is also weighted to the outer radius of 300–500 km where almost half of the drops are located. Some quadrants have a limited number of drops, for instance the left-rear quadrant within 150 km has only three drops. The distribution by radial distance and quadrant was assembled so that no one division contained ODWs from fewer than two hurricanes.

Different sampling strategies for the hurricanes present some minor problems. Dean has no ODWs inside of 250 km other than in the eye. Gabrielle only had a few deployments made inside of 500 km, all the other drops were 1000–1500 km ahead of the storm in a synoptic flow experiment, and Hugo has a disproportionate number of eye soundings. However, these problems are

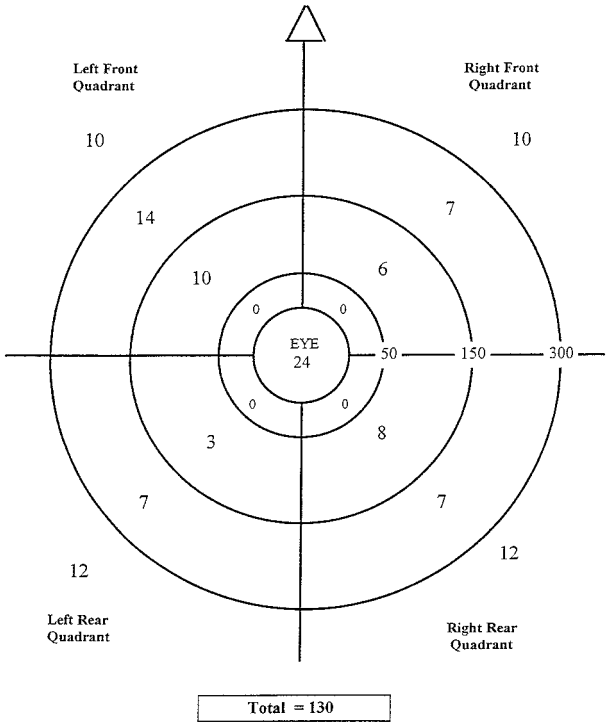

FIG. 2. Stratification of the 130 ODWs by radial distance and quadrant relative to storm motion (toward top of the page). The eye is the center. The circles represent ranges of 25–50, 50–150, 150–300, and 300–500 km. The numbers represent the ODWs dropped within that quadrant and radius.

inconsequential when compared to the potential impact of Hurricane Gustav (1990).

Over the course of three days, Gustav was sampled with a total of 44 successful ODW launches inside 500-km radius. In the region beyond 150 km, there are significant contributions made from the other five storms so the data are not overwhelmed by Gustav's inclusion. Inside of 150 km, Gustav accounts for one half of the ODW launches. To test the effect of Gustav, we ran all analyses we present here without Gustav data; the results are strikingly similar so we proceed with the entire dataset. See Bogner (1997) for the analyses excluding Gustav.

One of the problems in combining the six different hurricanes into one radial profile is the combining of weak and intense hurricanes. Based on the Saffir–Simpson scale of hurricane intensity, three of the storms are considered category one (CAT 1) hurricanes [Dean (1989), Gustav (day 1, 1990), and Iris (1995)], and three are category four (CAT 4) hurricanes [Luis (1995), Gabrielle (1989), and Hugo (1989)]. Hugo ranged from CAT 4 to CAT 5 during the three days of sampling. The first mission occurred when Hugo was a borderline CAT 5 hurricane and these drops were included in the CAT 4 analysis. Gustav was also a CAT 2 and 3 hurricane during two other sampling times. Based on this distribution, it was decided that an intensity stratification should be made with CAT 1 and CAT 4 hurricanes.

The ODWs from Dean, Iris, and those from the first day of Gustav are combined to represent a CAT 1 hurricane of 975–980 mb. The data from Gabrielle, Hugo, and Luis are combined to represent a CAT 4 hurricane of 935–940 mb. Data from Gustav are virtually eliminated from the sample (except for four CAT 1 drops) with the use of this stratification.

Studies of hurricane rainbands (Barnes et al. 1983; Barnes and Stossmeister 1986; Powell 1990a,b; Barnes and Powell 1995) illustrate that variations in thermodynamic and kinematic variables can be dramatic from the outer to the inner side of the band. Using this premise, the ODWs are categorized by their location relative to the reflectivity features of the primary rainband (both stratiform and convective regions), and the eyewall to determine variations in structure. Bands were labeled convective if they contained reflectivity maxima with a horizontal scale of 5–15 km. Such maxima are, of course, surrounded by a sharp reflectivity gradient and are interpreted as convective cells. Stratiform bands are those with a more homogeneous reflectivity field. To facilitate this stratification, lower fuselage radar scans, often from the WP-3D that was flying below the freezing level, were obtained for the time closest to the ODW launch to determine the location and conditions of the launch environment. Multiple scans minutes apart are used to examine the extent of attenuation and beam filling.

ODWs that are within 25 km of a rainband or the eyewall are separated out for identification of characteristics. Of the 106 ODWs launched outside of the eye, 31 are identified to be associated with rainbands and 4 are near, but not in, the eyewall. The 31 rainband ODWs are stratified by location (12 radially inside and 19 radially outside) and type of rainband (13 convective and 18 stratiform).

f. Data analysis and curve fitting

We wish to identify any trends in the data as a function of radial distance (x) from the storm center. Trends are determined by fitting a polynomial least squares curve to the data:

$$p(x) = c_1x^d + c_2x^{d-1} + \cdots + c_{n-1}x + c_n, \qquad (1)$$

where the degree is d and the number of coefficients is $n = d + 1$. The coefficients $c_1, c_2, \ldots, c_n$ are determined by solving a system of simultaneous linear equations. For each fitted polynomial curve, a measure of the goodness of fit (r^2) is calculated to determine how accurately the curve describes the variance within the data. We use polynomials of degrees two through four, which can represent nonlinear behavior. Changing the degree of the polynomial results in only small increases in the value of r^2 until many degrees are employed. For

example, the average increase in r^2 from degree one to degree two is 0.05, from degree two to degree three r^2 increases by 0.02, and from degree three to degree four r^2 increases by 0.01. Continually increasing the degree of the polynomial would eventually produce a curve that passes through every point, and has a perfect r^2, but this would be physically meaningless.

To produce the curves, we first calculate the means and standard deviations in 100-km range rings. Any value that is more than one standard deviation from the mean, and within 25 km of the radial endpoints, is eliminated. This is done because curve fits are more sensitive to the endpoints than points along the curve and thus require some refining to remove extremes. The curve is then generated but the r^2 value is determined for all the points.

When using the whole dataset of 130 values, a polynomial of degree three usually shows the trends. For a small set of 30 values, such as for the quadrant analysis, the degree was set to two. Fewer points coupled with a higher degree polynomial produces more physically unrealistic waves in the curve.

A large r^2 means the curve describes a substantial amount of the variance within the data. Additionally, the slope of each polynomial curve is subjected to a Student's *t*-test statistic. The null hypothesis is that the data are not a function of radial distance, that is, a horizontal line. This hypothesis is rejected at the 0.01 level of significance for all the variables we discuss.

g. Selection of an instability parameter

CAPE (Moncrieff and Miller 1976) currently serves as one of the standard measures of conditional instability:

$$\text{CAPE} = \int_{\text{LFC}}^{\text{EL}} g\frac{T_v - T_{ve}}{\overline{T_{ve}}}\,dz, \tag{2}$$

where T_v is the virtual temperature of the parcel, T_{ve} is the virtual temperature of the environment, and g is the gravitational acceleration. The integration is accomplished using a trapezoidal method for calculating the positive area and is performed from the level of free convection (LFC) to the equilibrium level (EL). The ascending parcel is characterized by the mean humidity and temperature in the lowest 500 m. Assumptions for its calculation include pseudoadiabatic ascent, no mixing with the environment, and we neglect the latent heat of fusion. There has been some debate whether ignoring the water loading leads to a gross overestimate of the instability, but Williams and Renno (1993) have shown that the negative effects of water loading in a reversible freezing process are more than countered by the latent heat of fusion. Estimating the amount of liquid water or the amount that undergoes freezing within an ascending parcel is challenging, even with the application of sophisticated radar techniques. For these reasons and since the prior work uses CAPE we will calculate it in the standard way.

Malkus (1952), Newton (1966), and LeMone et al. (1984) have shown that updrafts often have a large slope. CAPE remains a relevant parameter as long as the temperature field is homogeneous in the horizontal plane, as it typically is in the Tropics.

As a tropical cyclone spins up, the absolute angular momentum field develops with larger values found at greater radii. The quasi conservation of the angular momentum above the surface results in resistance to horizontal displacements; the consequence of this is that parcels in regions of large gradients of absolute angular momentum tend to ascend along a surface of constant angular momentum (M surface), rather than vertically. In this situation the calculation of slantwise convective available potential energy (SCAPE, e.g., Black et al. 1994) becomes a relevant parameter:

$$\text{SCAPE} = \int_{\text{LFC}}^{\text{EL}} g\frac{(\theta_e' - \theta_e)}{\overline{\theta_e}}\,dZ_M, \tag{3}$$

with θ_e' the equivalent potential temperature of the parcel; θ_e the equivalent potential temperature of the environment; $\overline{\theta_e}$ the mean through the depth, dZ_M; and g the gravitational acceleration. The integration is done along an M surface.

SCAPE would have little impact on the calculation of instability if the temperature or θ_e was homogeneous in the horizontal plane. In a mature hurricane these fields contain strong horizontal gradients, especially aloft, where there is a prominent warm core (e.g., Hawkins and Imbembo 1976). As an M surface tilts outward the parcel would have greater SCAPE because it is moving through a cooler environment aloft than it would near the warm core. The question that now arises is: Does a parcel follow an M surface? The numerical simulation of an axisymmetric tropical cyclone by Rotunno and Emanuel (1987) shows that the slopes of the M surfaces in the radial direction near the eye are from 45° to 90°, but by 75 km radial distance the slope is about 5°, and by 150 km it is 3°. Updrafts may have slopes as small as 20° (see the aforementioned updraft slope papers) but they do not follow the extremely shallow slopes of the M surfaces estimated by Rotunno and Emanuel (1987) that are found farther from the eye. Other than inside the eye, we have no soundings until we reach 75-km radial distance. Given that we have virtually no soundings that would describe conditions near the eye we have foregone the use of SCAPE.

3. Results

a. Conditional instability below 500 mb

ODW deployment levels vary between 400 and 500 mb. For this reason, all ODWs are truncated at 500 mb (the equilibrium level is forced to 500 mb by inserting a strong inversion) to create a common level for an

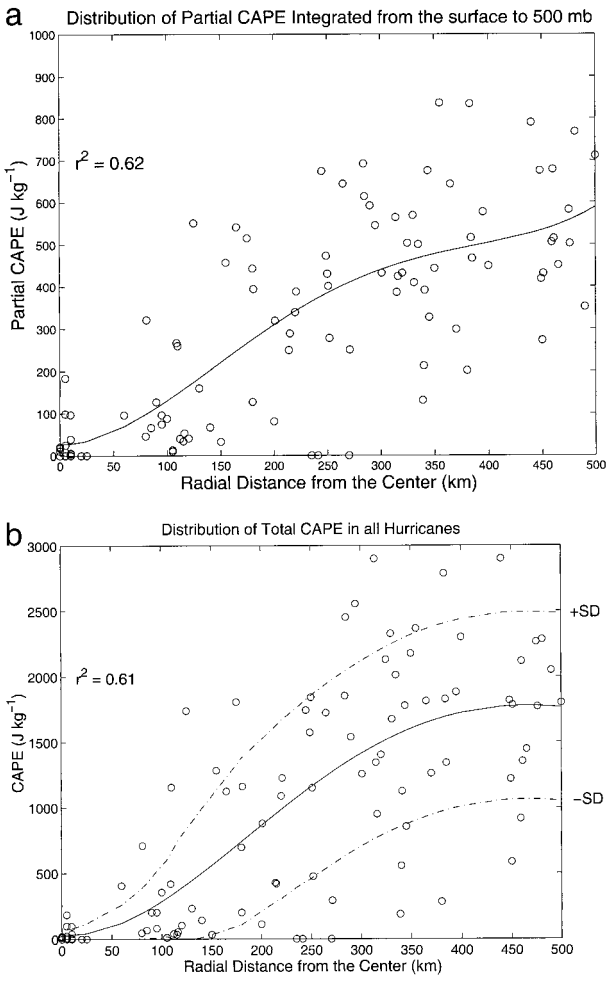

FIG. 3. (a) The radial distribution of PCAPE below 500 mb. (b) The radial distribution of total CAPE in all hurricanes as a function of radial distance. The line represents a polynomial curve fit to the data; measure of fit is indicated by the r^2 value. Plus or minus one standard deviation (±SD) from the range-dependent mean is also shown in (b) with the dashed lines. Open circles represent the values calculated for each ODW.

analysis of the partial CAPE (PCAPE). There is considerable scatter among the PCAPE values (Fig. 3a) at all radii, which does not diminish for any particular hurricane. PCAPE is shown to decrease radially inward from 600 J kg^{-1} at 500 km to 100 J kg^{-1} at 100 km. The eye contains essentially no PCAPE (~20 J kg^{-1}). The fitted curve describes the data reasonably with an $r^2 = 0.62$.

b. Conditional instability of the total sounding

CAPE for the full sounding (Fig. 3b) indicates that substantial amounts of conditional instability exist in the regions outside of 300 km where the values average 1500–1700 J kg^{-1}. While these values may seem high for the hurricane environment, CAPEs in the environments of other tropical convective systems have comparable values. Zipser and LeMone (1980) found CAPE averaged 1500 J kg^{-1} in the environment surrounding eastern Atlantic cumulonimbi during the Global Atmospheric Research Program (GARP) Atlantic Tropical Experiment (GATE). CAPE values determined by Alexander and Young (1992) for six tropical squall lines north of Australia averaged 1800 J kg^{-1} and four nonsquall cases averaged 1700 J kg^{-1}. Griffith (1993) arrived at a value of 1800 J kg^{-1} for eight squall line cases in the same region. It is important to note that roughly two thirds of the CAPE at 500 km is accounted for with the added sounding top. However, this ratio is similar to the results obtained by halving soundings from fast and slow moving convective lines sampled during GATE (Barnes and Sieckman 1984). Most tropical soundings have a fairly constant virtual temperature excess through most of the troposphere.

Inside of 300 km, the values of CAPE decrease rapidly and approach near-neutral conditions inside of 100 km, near the eyewall. This result suggests that eyewall convection may be fundamentally different from the convection occurring at larger radii within the rainbands. Evidence for this is the detection of updrafts of relatively modest strength (5–6 m s^{-1}) on virtually every pass made by aircraft through the eyewall (e.g., Jorgensen 1984a,b), suggesting that at least some hurricanes could be modeled as a mesoscale ring of ascent rather than a series of cumulonimbi. In the latter case one would expect to sample downdrafts or quiescent conditions at least for some passes like those through rainbands (e.g., Barnes et al. 1983).

CAPE is effectively reduced within 300 km of the center (from 1500 to ~200 at 75 km) by a combination of upper-level warming and lower-level cooling. A comparison of mean temperature profiles at 100 km (includes drops from 75 to 125 km) and 500 km (includes drops from 450 to 500 km) radius (Fig. 4) indicates that the profile increasingly evolves toward moist adiabatic above a shrinking dry-adiabatic mixed layer. The mean 500-mb temperatures for 100 km average ~4°C warmer than those found at 400–500 km. Meanwhile, temperatures in the lowest 500 m cool by nearly 3°C from 500 to 100 km. This trend toward lower CAPE is decisively downward with an $r^2 = 0.61$. However, similar to the PCAPE values, there is a large amount of scatter associated within the CAPE values at any given radius.

All ODWs with CAPE values exceeding one standard deviation from the range-dependent mean were examined to learn why they were so far from the fitted curve (Fig. 3b). A total of 24 soundings outside the eye were noted, including 13 larger and 11 smaller than one standard deviation from the curve. Small CAPE soundings exhibited much drier surface conditions with mixing ratios of ~15 g kg^{-1} as opposed to ~18 g kg^{-1} for the large CAPE soundings. Temperatures in the small CAPE instances are determined to be cooler at the surface (~1°C) than the large CAPE soundings and warmer at 500 mb by 1°C. Large CAPE soundings are associated

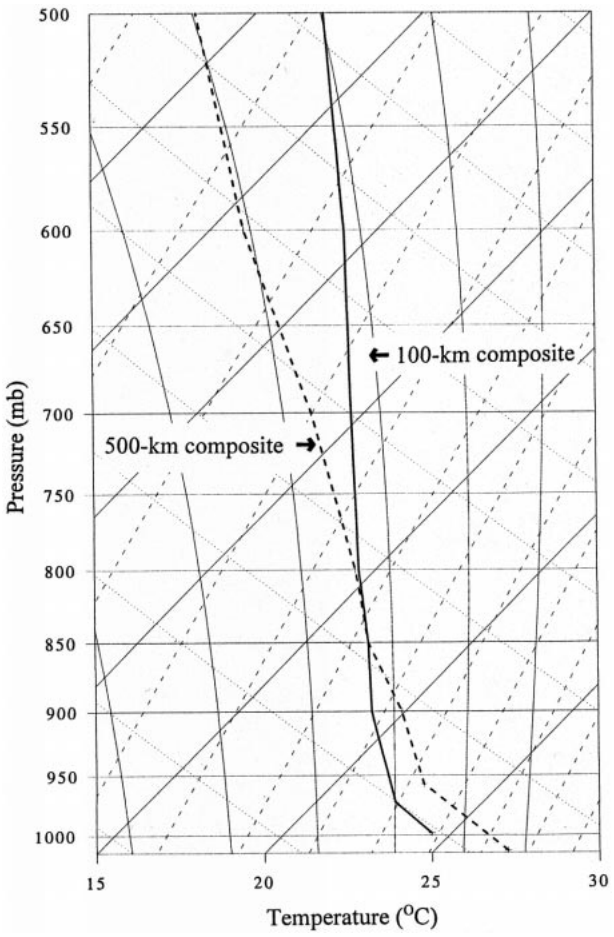

FIG. 4. Mean temperature profiles for 500-km radius (dashed line) and for 100 km (solid line).

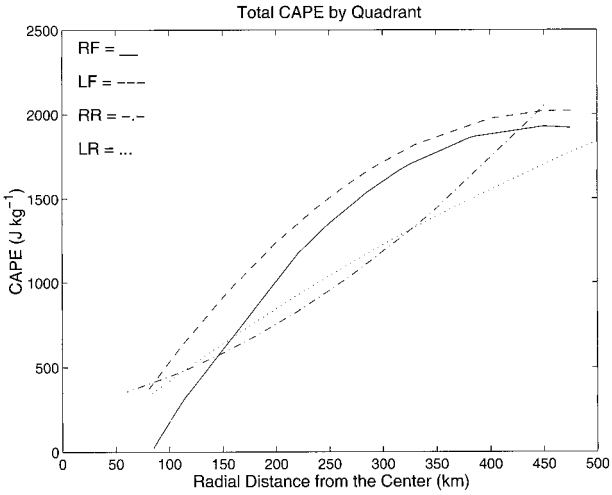

FIG. 5. Fitted curves for CAPE by quadrant as a function of radius. Quadrant trends follow this convention: right front (solid), left front (dashed), right rear (dash–dot), and left rear (dotted).

with clear regions, based on radar, whereas the small CAPE soundings are found within convectively modified air consistent with convective wake or anvil soundings identified by Zipser (1977), Barnes et al. (1983), and Powell (1990a).

Quadrant to quadrant analysis (Fig. 5) depicts a similar decrease of CAPE versus radius within each quadrant. The variations in CAPE are not large with differences of only 100–300 J kg^{-1} among the quadrants. There is slightly more CAPE in the left and right front quadrants (~200 J kg^{-1}), but these tropical cyclones (TCs) are better described as approximately axisymmetric.

Stratifying the hurricanes by intensity reveals that the CAT 1 hurricanes (Fig. 6, upper panel) have a weakly defined radial trend in CAPE, with values at 100-km radius comparable to those found at 500-km radius. The nearly flat curve fit is due to the large amount of scatter exhibited in CAT 1 hurricanes, which is indicated by an $r^2 = 0.38$. However, the CAT 4 hurricanes display a strong downward trend with decreasing radius (Fig. 6, middle panel) and less scatter than CAT 1 storms ($r^2 = 0.67$). The lower panel of Fig. 6 demonstrates that the two categories are in contrast. Inside of 240 km, the primary difference between the two is found to be the magnitude of the warm core. Temperatures in the CAT

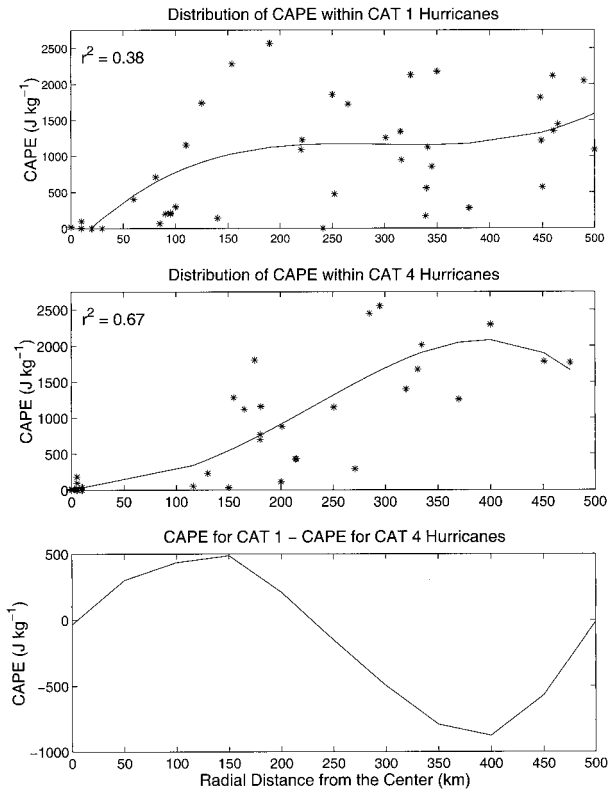

FIG. 6. Distribution of CAPE by intensity of hurricane. CAPE is shown for CAT 1 hurricanes (top), CAT 4 hurricanes (middle), and the difference between the two categories, CAT 1–CAT 4 (bottom). Convention is the same as in Fig. 3b.

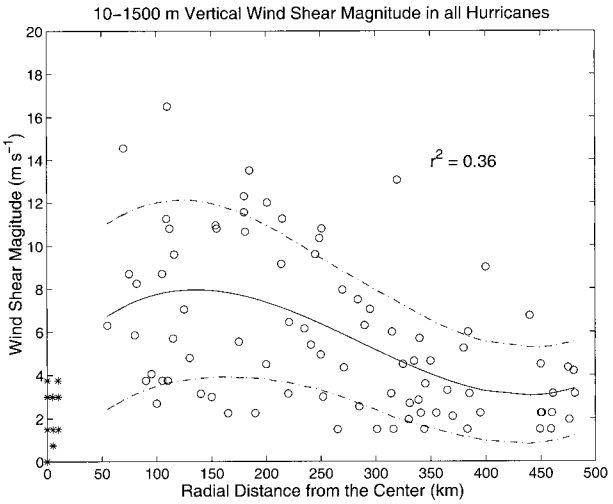

FIG. 7. Distribution of 10–1500-m vertical wind shear magnitude as a function of radial distance from the center. Convention is the same as in Fig. 3b. The stars represent shear values in the eye.

4 storms at 500 mb, within 100–200 km, are found to be as much as 2°C warmer than in CAT 1 storms, supporting smaller CAPEs for the CAT 4 storms near the center. Contributing to the decreased instability is the greater cooling of the inflow within the CAT 4 hurricanes. Beyond 240–500 km, the CAT 4 storms have more CAPE. We note that at large radii there are fewer soundings within CAT 4 storms exhibiting structure evocative of disturbed or overturned conditions.

CAPE is correlated with the type of rainband found nearby. Stratiform bands have smaller CAPE values with 700 J kg^{-1} radially outward of and 300 J kg^{-1} radially inward of the bands while convective bands have larger CAPE of 1100 J kg^{-1} radially outward and 500 J kg^{-1} radially inward. It is not surprising that the CAPE for the convective bands would be higher since larger instability allows for stronger vertical motions. The stratiform bands are most often located in areas associated with subsidence such as that found in anvil precipitation (e.g., Gamache and Houze 1982). From this stratification, we find that soundings radially inside of rainbands (stratiform or convective) are most likely to contain the lowest CAPE values while radially outside of the bands CAPEs are likely to be significantly higher; however, these CAPEs are not as high as those soundings made far from any reflectivity features.

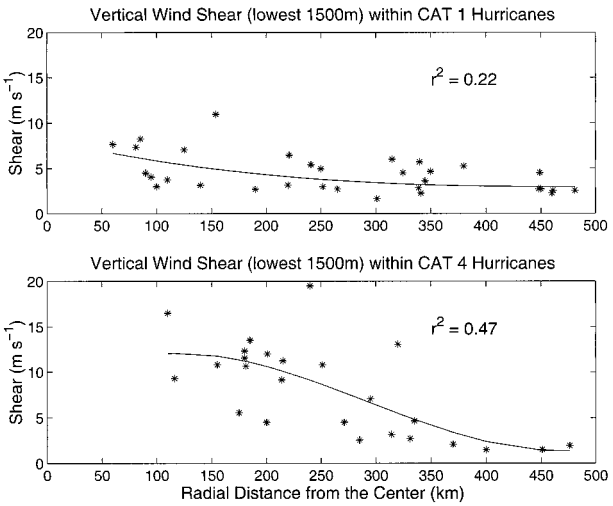

FIG. 8. Distribution of the 10–1500-m vertical wind shear magnitudes for (top) CAT 1 hurricanes and (bottom) CAT 4 hurricanes as a function of radial distance from the hurricane center.

c. The 1500-m vertical shear

Novlan and Gray (1974) identified a threshold vertical shear of the horizontal wind from the surface to 850 mb that was correlated with tornadogenesis in hurricanes. Consequently, a similar shear value was calculated over the first 1500 m of each ODW profile by taking $\partial v/\partial z$ from the 10-m estimate to the 1500-m ODW wind observation.

Wind shear magnitudes (Fig. 7) increase from 2 to 3 m s^{-1} per 1500 m (1.7×10^{-3} s^{-1}) at 500 km to a maximum of 8–9 m s^{-1} per 1500 m (5.7×10^{-3} s^{-1}) by a radius of 100 km. Shear magnitudes exhibit a steady increasing trend with a curve fit of $r^2 = 0.36$. It is apparent that the scatter increases as the radius decreases in toward the eye. A stratification by quadrant did not reveal any important differences. The small shear variations between quadrants indicate that the hurricane has a nearly axisymmetric low-level wind field over the ocean.

The distribution of shear as a function of radius for CAT 1 hurricanes (Fig. 8, top panel) displays small variations with magnitudes increasing from 2 to 5 m s^{-1} per 1500 m (1.3 to 3.3×10^{-3} s^{-1}) as radius decreases. However, CAT 4 hurricanes (Fig. 8, lower panel) exhibit a strong upward trend with less scatter ($r^2 = 0.47$). Shear magnitudes increase dramatically from 2 m s^{-1} per 1500 m at 500-km radial distance to 12–13 m s^{-1} per 1500 m (8.3×10^{-3} s^{-1}) by 150 km. The large shears in the CAT 4 storms are a result of a much stronger 1500-m wind maximum than for the CAT 1 storms. Sample wind profiles at 175-km radius for a CAT 4 hurricane (Luis) and CAT 1 hurricane (Iris) (Fig. 9) demonstrate the difference in the wind maxima.

Values beyond the plus or minus one standard deviation envelope of the shear magnitude through the 1500-m layer (Fig. 7) are separated out to identify common properties. All of the 13 extreme high-shear cases are attributed to CAT 3 and CAT 4 hurricanes. Of the 11 extreme low-shear cases, 8 are associated with CAT 1 hurricanes and the remaining 3 are within CAT 4 hurricanes located radially inward from convective rainbands. Intensity is the primary controller of the scatter within the shear values; however, proximity to rainbands

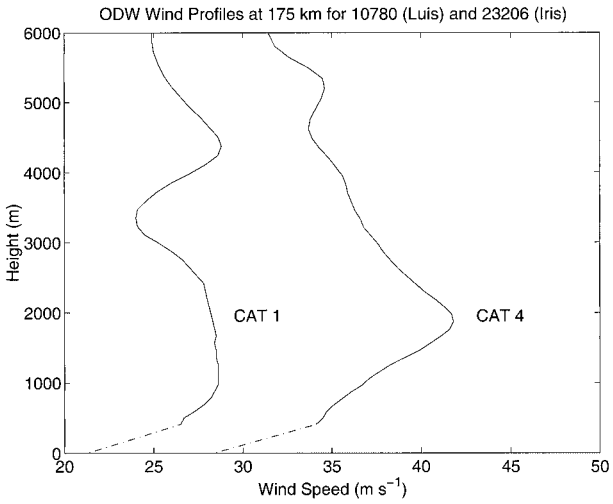

FIG. 9. Example of an ODW wind profile for Iris (1995), a CAT 1 hurricane, and Luis (1995), a CAT 4 hurricane. The dash–dot line represents the wind correction to the 10-m level.

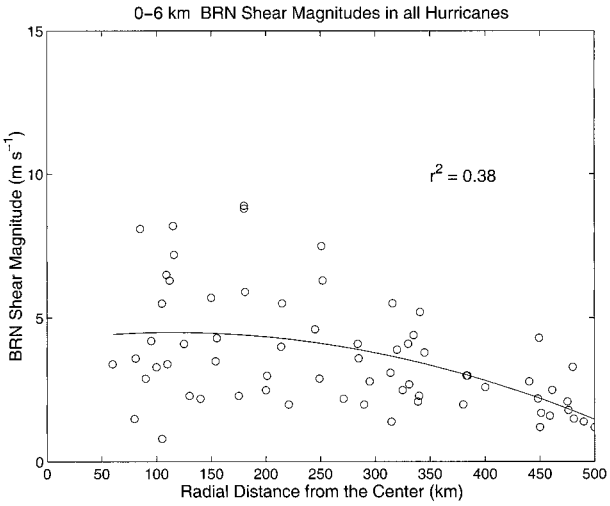

FIG. 10. Distribution of the magnitude of the 0–6-km density-weighted vertical shear (BRNS) as a function of radial distance from the storm center. Convention is the same as in Fig. 3b.

is a contributing factor. Of the 13 extreme high shears, all are located near stratiform rainbands.

The reflectivity stratification used for CAPE was re-examined for vertical shear. Stratiform rainbands average a magnitude of 8.4 m s^{-1} per 1500 m (9.8 m s^{-1} radially inward and 6.8 m s^{-1} radially outward) while convective bands average 3.5 m s^{-1} per 1500 m (3.3 m s^{-1} radially inward and 3.8 m s^{-1} radially outward). Lower shears within convective bands are likely caused by stronger winds at the surface, which are mixed down by the convective downdrafts.

The uncertainty of the 10-m winds, based on the work of Powell (1980), is about 10%. This will vary our shear estimates by a little less than 1.5×10^{-3} s^{-1}. We have no reason to assume that the behavior of the 10-m wind for our measurements differs from those analyzed by Powell (1980), and note that the increase of shear with decreasing radius is much larger than the uncertainty that we face.

d. Bulk Richardson number and shear

The bulk Richardson number (BRN) is the ratio between the buoyancy and the vertical shear:

$$\text{BRN} = \frac{\text{CAPE}}{0.5(\mathbf{V}_{10\text{–}6000m} - \mathbf{V}_{10\text{–}500m})^2}, \qquad (4)$$

where CAPE is the buoyancy throughout the troposphere (positive area on a thermodynamic diagram), $\mathbf{V}_{10\text{–}6000\text{m}}$ represents the density weighted mean wind from 10 to 6 km, and $\mathbf{V}_{10\text{–}500\text{m}}$ represents the mean wind in the lowest 500 m. The term in parentheses is often referred to as the bulk Richardson number shear (BRNS). This calculation scheme follows that developed by Weisman and Klemp (1982) and used by McCaul (1991) and has become a regularly calculated parameter by the National Weather Service.

The ratio has been shown to be a useful forecasting tool in predicting the type of thunderstorm activity (e.g., supercell or multicell thunderstorms). Weisman and Klemp (1982, 1984) determined through modeling and case studies that types of convection can be classified by ranges of BRN values. They determined that BRN values larger than 40 are most often associated with multicell thunderstorms and values ranging from 10 to 40 correspond well to supercell convection. Within the modeling studies that use simple wind profiles, it is further demonstrated that the nature of convection is largely a function of the 0–6-km vertical shear. Since the occurrence of tornadoes is often linked to supercell convection, it is useful to locate those regions where the environment favors this type of convection.

The BRNS magnitudes (Fig. 10) gradually increase from 1.5 m s^{-1} [here we report shear following the style of McCaul (1991)] at 500 km to 5 m s^{-1} by 150 km. The scatter also increases ($r^2 = 0.35$) and a large range in BRNS can be seen nearing the eyewall. The scatter exhibited similar properties to those found for the 1500-m vertical shear. Unlike the shears estimated over the lowest 1500 m, the BRNS shows more of an asymmetric distribution (Fig. 11) with the right-front quadrant having the largest shear magnitude and the left rear the lowest by about 3–4 m s^{-1}. The mean-storm relative hodographs for each quadrant (Figs. 12a–d) show that the near-axisymmetric wind field develops a large asymmetry in the right semicircle as the right-front and right-rear quadrants display an open ''horseshoe'' signature indicating a larger variation in wind direction as winds veer almost continuously with height; the left-front (LF) and especially the left-rear quadrants close in upon themselves as the winds first veer, then back, with

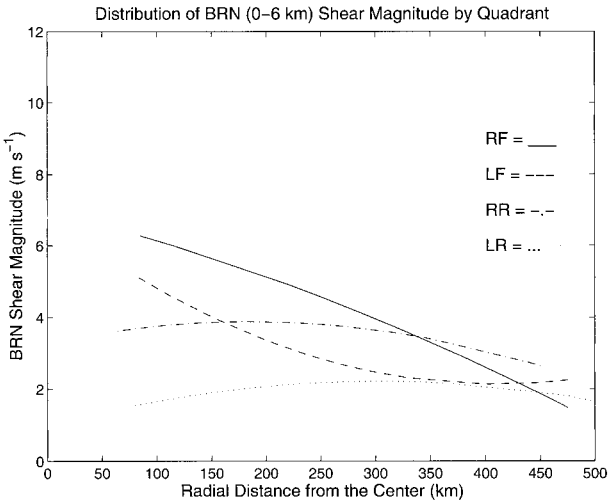

FIG. 11. The fitted curves for BRNS as a function of quadrant and radius. Plotting convention follows Fig. 5.

height. This asymmetry may be a result of the superposition of the shear within the environmental steering flow upon the hurricane circulation (McCaul 1991). Higher values of BRNS are associated with the more intense CAT 4 hurricanes as values increase from 2 m s^{-1} at 500 km to around 8 m s^{-1} by 150 km; CAT 1 hurricanes have a fairly flat trend from 2 to 4 m s^{-1} over the same distance.

As might be expected from the CAPE and BRNS values, bulk Richardson numbers (Fig. 13) show a strong downward trend with decreasing radius ($r^2 = 0.52$). Values initially average 200–300 at 400–500-km radius but decrease to the 10–40 range inside of 250 km. The average values outside of 250 km are typically associated with multicellular convection but at any given radius there are areas where the combination of CAPE and shear will produce low bulk Richardson numbers. The combination of increasing BRNS and decreasing CAPE creates a favorable region within 250 km for supercell convection as the bulk Richardson numbers fall in the 10–40 range. However, it must be pointed out that a BRN in the 10–40 range does not mean a tornado will form; it just indicates that conditions are favorable for supercell convection.

Although not all tornadoes occur from supercells, a recent study using Doppler radar has shown that tornado occurrences within Tropical Storm Gordon (1994) and Hurricane Allison (1995) had origins within shallow supercells that exhibited small mesocyclones up to 30 min before tornadogenesis and lasting for 1–2 h (Spratt et al. 1997). This observation is consistent with model simulations of shallow hurricane supercells (McCaul and Weisman 1996), which show cell tops lower than 6-km height with a peak updraft near 2 km accompanied by a small diameter mesocyclone, strongest at 1.5-km height.

e. Total cell relative helicity

Lazarus and Droegemeier (1990) have argued that BRNS is a poor predictor of tornado formation because it does not describe the complete wind profile, namely the low-level curvature shear. To further determine the ability of a hurricane supercell to support possible waterspout genesis, it is necessary to assess the ability of the environment to create rotation in the thunderstorm and associated updraft. Cell-relative total helicity combines storm motion with streamwise vorticity, which, when tilted vertically within the updraft, induces rotation. Lilly (1986) and Wu et al. (1992) describe the flow within a supercell updraft as primarily helical and suggest that helicity acts to reduce the effects of turbulence on supercell updrafts allowing for their prolonged steady state. Davies-Jones et al. (1990) indicate that environmental helicity shows promise as a tool for predicting tornadogenesis. The cell-relative total helicity (H_t) for each ODW is calculated in the same manner as McCaul (1991) using the equation defined by Lilly (1986):

$$H_t = (\mathbf{V} - \mathbf{V}_c) \cdot (\mathbf{k} \times \partial\mathbf{V}/\partial z), \qquad (5)$$

where $\mathbf{V}$ is the ground-relative flow, $\mathbf{V}_c$ is the cell motion, $\mathbf{k}$ is the unit vector in the vertical (z) coordinate, and $\partial\mathbf{V}/\partial z$ is the shear. Here, $\mathbf{V}_c$ is not known because reflectivity information is not available frequently enough to track the cell. However, an estimate can be obtained by calculating the 0–6-km mass-weighted mean wind for the sounding. The problem is that cell motions can have large deviations from the mean wind making these helicity estimates only approximations of the true helicity values (McCaul 1991).

The total helicity (Fig. 14) increases gradually with decreasing radius, but the curve fit is poor. Values initially of 0.005 m s^{-2} at 500 km rise to 0.02 m s^{-2} by 150 km. Converting these values to the form used by Davies-Jones et al. (1990), by multiplying by the averaging depth of 3000 m, reveals helicities of only 15 m^2 s^{-2} at 500 km increasing to only ~60 m^2 s^{-2}. These values are significantly less than the threshold value for tornado formation of 160 m^2 s^{-2} suggested by Davies-Jones et al. (1990).

4. Comparison to overland observations

a. CAPE

The distribution of CAPE within the hurricane over land was shown by McCaul (1991). The land environment is asymmetric with the largest instability found on the right side of the circulation. Instabilities to the left of the hurricane track are only half of those seen in the right semicircle. This asymmetry is produced by the hurricane circulation interacting with the cooler, drier air modified by land; over the ocean the distribution of CAPE is approximately axisymmetric. For both environments CAPE decreases inward toward the center.

CAPE values do show differences at distances beyond

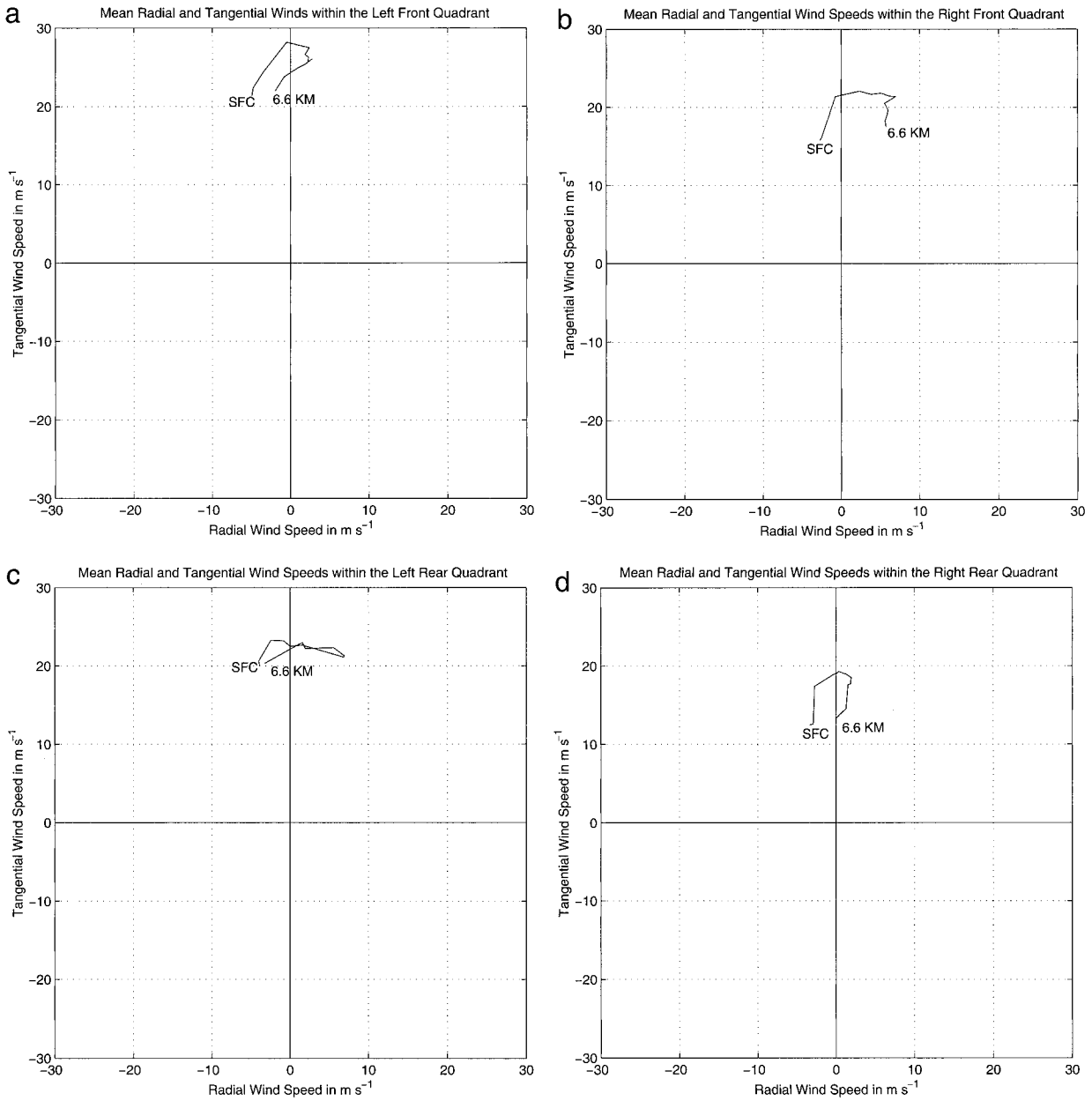

FIG. 12. Mean quadrant hodographs plotted as a function of radial wind (V_r) and tangential wind speeds (V_θ). Quadrants are relative to a storm moving northward (0°) with (a) left-front quadrant, (b) right-front quadrant, (c) left-rear quadrant, and (d) right-rear quadrant. Wind increments are every 10 m s^{-1}.

250-km radius between land and sea soundings. Values over the land at 400–500 km radius average 1200–1400 J kg^{-1} within the right semicircle, which is 300–400 J kg^{-1} lower than those over the ocean. These lower CAPEs are the result of cooler land temperatures (about 1.5°C less than the ocean) and less moisture (~1 g kg^{-1}) in the boundary layer. CAPE over land within the left semicircle is always less than the values found over the ocean except near the center. Once inside of 250 km, our values for the oceanic environment are very close to those found by Sheets (1969) and McCaul (1991). The mean hurricane sounding of Sheets (1969) contains 680 J kg^{-1} at an average distance of 150 km, which is similar to oceanic CAPE values at this radius. Individual CAPE values for the five Sheets composites based on pressure, which can be interpreted as distance from the eye, show a downward trend with values nearly identical to what we observe.

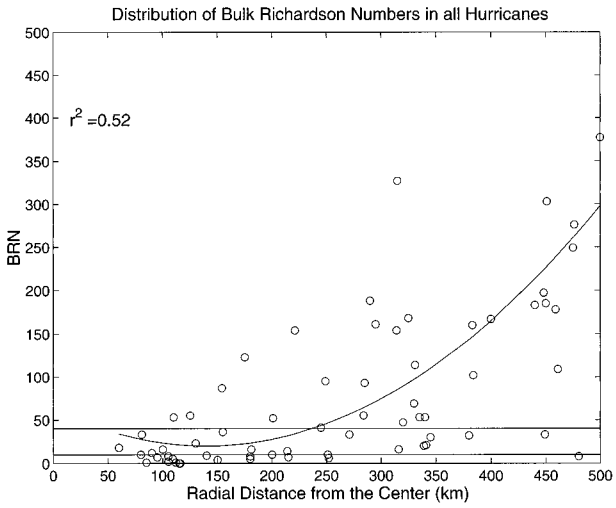

FIG. 13. Distribution of BRN as a function of radial distance from the storm center. The range for supercell convection (10–40) is indicated by the horizontal bars. Plotting convention is the same as in Fig. 3b.

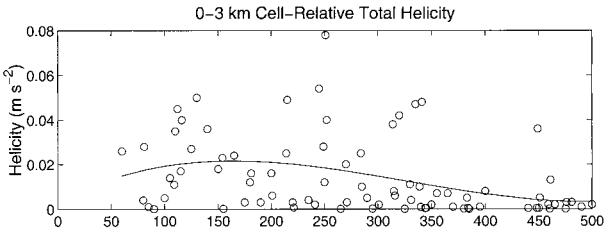

FIG. 14. Distribution of the cell-relative total helicity as a function of radial distance from storm center. The plotting convention is the same as in Fig. 3b.

b. The 1500-m and 0–6-km vertical wind shears

Vertical shears within the land environment were described in detail by Novlan and Gray (1974) and McCaul (1991). Novlan and Gray defined a threshold vertical shear of 20 m s^{-1} from the surface to 850 mb that is associated with tornadogenesis in the right-front quadrant of hurricanes. Hurricanes that did not produce tornadoes averaged surface to 1500 m vertical shears of 12–14 m s^{-1}. Over the ocean, the 1500-m vertical shears are shown to be significantly less with the highest average shears approaching only 8 m s^{-1} inside of 150 km. In the region 200–400 km from the center at which the threshold value was defined, the values average only 3–7 m s^{-1} per 1500 m. Shear values over the ocean are approximately one half of the land values with the maximum occurring closer to the center.

The density weighted 0–6-km vertical shear (BRNS) magnitudes are calculated by McCaul (1991) for the land environment of the hurricane. A maximum BRNS magnitude of 10 m s^{-1} is found on the right side of the hurricane between 200 and 400 km. This asymmetry of BRNS over land matches the ocean environment where the right semicircle has more speed and more of a directionally sheared environment than the left-front quadrant. This asymmetry is likely the result of the superposition of the steering flow onto the hurricane circulation. BRNS magnitudes over the ocean are only one half of those over land with the maximum reaching only 5 m s^{-1} by 150 km. These large differences suggest that abrupt changes are occurring within the vertical profiles of the horizontal wind at landfall. Examples of how quickly these changes occur at landfall are found in Powell and Houston (1996), Powell et al. (1998), and Houston et al. (1997). They use oceanic reconnaissance level winds reduced to 10 m and land station wind observations corrected to open exposure and 10 m to demonstrate that the winds are reduced by 7–10 m s^{-1} near the coastline.

A direct comparison of ODW and rawinsonde measured shears is beyond the capability of this dataset. Only one of the six hurricanes [Hugo (1989)] made landfall on the U.S. coastline. Unfortunately, all of the ODW deployments outside of the eye occurred five days earlier while Hugo was still in the Caribbean. McCaul (1991) describes Hugo, which produced two reported tornadoes, as possessing strong boundary layer wind shear after landfall. The Greensboro, North Carolina, sounding located to the right of the storm track showed 45 m s^{-1} at 850 mb and 20 m s^{-1} at the surface almost 12 h after landfall. It is interesting to note that five days previous, when Hugo was at its peak intensity, the largest shears were less than half of the 25 m s^{-1} observed after landfall.

c. Bulk Richardson numbers and helicity

BRN values that favor supercells for the land environment are located within the semicircle to the right of the storm track at a radius of 200–400 km (McCaul 1991). At sea, hurricanes are similar in that they too reach the supercell criteria within the two right quadrants, however, there are two main differences in the BRN distributions. Over the ocean, the BRN supercell criterion is reached in all quadrants of the hurricane and the preferred BRN range for supercell formation occurs closer ($<$250 km) to the center of circulation. Occurrences of supercells near and in the eyewall observed during reconnaissance missions have been described by Black et al. (1986) and Black and Marks (1991).

The calculations for cell-relative total helicity by McCaul (1991) show a maximum in the right semicircle of the hurricane circulation at a radius of 200–400 km over land. Ocean values have a maximum in the same quadrants but the location is closer (within 200 km). The difference is that while maximum land magnitudes exceed 0.04 m s^{-2} (helicity through a depth of 3000 m $= 120$ m^2 s^{-2}), the maximum ocean values relax to 0.02 m s^{-2} (60 m^2 s^{-2}). Similar to the trends in vertical shear, the cell-relative total helicity is roughly one half of the land values within tornadic hurricanes.

Table 2 is a summary of the differences and similar-

TABLE 2. Summary of stability parameters within the hurricane land and ocean environments. Maximum values and corresponding radial distances from storm center for the various stability and shear parameters within the hurricane environment over the land and over the ocean. A further stratification by intensity within the ocean environment is represented by CAT 1 and CAT 4.

Variable max value and radial distance	Land	Ocean	Ocean CAT 1	Ocean CAT 4
CAPE	1200–1400 J kg^{-1}	1500–1700 J kg^{-1}	1500 J kg^{-1}	2000 J kg^{-1}
	300–500 km*	300–500 km	400–500 km	375–450 km
10–1500-m vertical shear	20 m s^{-1} tornadic,	8.5 m s^{-1}	6 m s^{-1}	12.5 m s^{-1}
	13 m s^{-1} in nontornadic TC	75 km	75 km	150 km
	200–400 km**			
10–6000-m BRN shear	10 m s^{-1}	5 m s^{-1}	4 m s^{-1}	8 m s^{-1}
	200–400 km*	150 km	150 km	150 km
Cell-relative total helicity (m s^{-2})	0.04 m s^{-2}	0.02 m s^{-2}	0.015 m s^{-2}	0.03 m s^{-2}
	200–400 km*	150 km	100 km	125 km

* Observed values obtained from McCaul (1991).
** Observed values obtained from Novlan and Gray (1974).

ities between our oceanic measurements and the overland measurements discussed by McCaul (1991) and Novlan and Gray (1974).

5. Conclusions

Vertical thermodynamic and kinematic structures within 500 km of six Atlantic hurricanes are determined using 130 ODW observations. The ODW data require adjustments to estimate mixed layer mixing ratio and surface wind speed, and a sounding top must be attached to the ODW data to complete the profile to the tropopause. ODW distributions are checked for hurricane to hurricane biases; no serious compromises are found.

CAPE, a measure of the atmosphere's conditional instability, is found to have a maximum of 1500–1700 J kg^{-1} at large radii. Inside a 300-km radius, CAPE values decrease from 1500 to ~200 J kg^{-1} by 75-km radius. CAPE decreases in response to upper-tropospheric warming and boundary layer cooling. This decrease is larger for CAT 4 hurricanes than for CAT 1 hurricanes. The variations of CAPE between quadrants are small, which supports an axisymmetric approximation. Analysis of CAPE below 500 mb, which does not include any assumptions about the temperatures above aircraft altitude, verifies these results. Comparisons with the environment over land shows values within 250 km of the circulation center are nearly identical, but beyond 250 km CAPE is larger by 300–400 J kg^{-1} over the ocean.

The magnitude of the vertical shear in the lowest 1500 m increases from 2 m s^{-1} at 500 km to 8.5 m s^{-1} by 75 km. Magnitudes for the 0–6-km vertical shear increase from 1.5 m s^{-1} at 500 km to 5 m s^{-1} by 75 km. Mean quadrant hodographs indicate that the right-front quadrant contains the largest speed and directional shears of all the quadrants with the left rear having the least. Scatter within the 1500-m and 0–6-km shear is strongly dependent on the intensity of the hurricane. In both cases, the vertical shear is half the magnitude observed over land, supporting the hypothesis that large changes in the vertical wind structure occur at landfall.

CAPE and 0–6-km vertical shear are primary environmental factors used to forecast thunderstorm type via the bulk Richardson number. The belt of BRN values associated with the possibility of supercells (10–40) is found to occur within 75–250 km from the circulation center. While bulk Richardson numbers support supercells, cell-relative total helicity measurements increase from 15 m^2 s^{-2} at 500 km to only 60 m^2 s^{-2} by 150 km. These values are also one half of the helicity measured over the land and significantly lower than the suggested threshold value of 160 m^2 s^{-2} for tornadogenesis. This suggests that supercells may exist within 250 km of the hurricane center, but their ability to produce strong waterspouts is low. At landfall the shears appear to be enhanced considerably leading to an increase in the success rate of tornadogenesis.

The CAPE trends we diagnose are consistent with the cloud to ground lightning flash rate patterns observed in hurricanes (Molinari et al. 1994, 1999). They found fewer flashes in the inner 100 km for higher category hurricanes than for the weaker hurricanes; this may be attributed to a lack of supercooled water and/or a lack of strong updrafts. Weaker updrafts would of course result from lower CAPE. Our CAT 4 composite has a greater reduction in CAPE as one approaches the eyewall than does the CAT 1 composite. Molinari et al. (1999) also found a rapid increase in the flash rate beyond 130–190-km radius. We find this to be where CAPE rapidly increases with increasing radius, presumably because this is a typical outer extent for the subsidence/moat region. They also found high flash rates for outer rainbands that propagate outward, again this is where these bands would tap higher CAPE if our results are representative of the typical situation.

Acknowledgments. This research was conducted with support from NSF Grant ATM97-14410, NOAA Atlantic Oceanographic and Meteorological Laboratory, Hurricane Research Division, and the Joint Institute for Marine and Atmospheric Research, University of Hawaii.

We would like to thank John Molinari and Pat Fitzpatrick for reviews that improved the manuscript.

REFERENCES

Alexander, G. D., and G. S. Young, 1992: The relationship between EMEX mesoscale precipitation feature properties and their environmental characteristics. *Mon. Wea. Rev.,* **120,** 554–564.

Barnes, G. M., and K. Sieckman, 1984: The environment of fast- and slow-moving tropical mesoscale convective cloud lines. *Mon. Wea. Rev.,* **112,** 1782–1794.

——, and G. J. Stossmeister, 1986: The structure and decay of a rainband in Hurricane Irene (1981). *Mon. Wea. Rev.,* **114,** 2590–2601.

——, and M. D. Powell, 1995: Evolution of the inflow layer of Hurricane Gilbert (1988). *Mon. Wea. Rev.,* **123,** 2348–2368.

——, E. J. Zipser, D. Jorgensen, and F. Marks Jr., 1983: Mesoscale and convective structure of a hurricane rainband. *J. Atmos. Sci.,* **40,** 2125–2137.

Black, P. G., and F. D. Marks Jr., 1991: The structure of an eyewall meso-vortex in Hurricane Hugo (1989). Preprints, *Conf. on Hurricanes and Tropical Meteorology,* Miami, FL, Amer. Meteor. Soc., 579–582.

——, ——, and R. A. Black, 1986: Supercell structure in tropical cyclones. Preprints, *Joint Sessions 23d Conf. on Radar Meteorology Conf. on Cloud Physics,* Vol. 3, Snowmass, CO, Amer. Meteor. Soc., JP255–JP259.

Black, R. A., H. B. Bluestein, and M. L. Black, 1994: Unusually strong vertical motions in a Caribbean hurricane. *Mon. Wea. Rev.,* **122,** 2722–2739.

Bogner, P. B., 1997: Conditional instability and shear within hurricanes over the ocean. M.S. thesis, Dept. of Meteorology, University of Hawaii, 94 pp. [Available from Dept. of Meteorology, University of Hawaii, Honolulu, HI 96822.]

Davies-Jones, R. D., D. W. Burgess, and M. Foster, 1990: Test of helicity as a tornado forecast parameter. Preprints, *16th Conf. on Severe Local Storms and Conf. on Atmospheric Electricity,* Kananaskis Park, AB, Canada, Amer. Meteor. Soc., 588–592.

Frank, W. M., 1977: The structure and energetics of the tropical cyclone. I. Storm structure. *Mon. Wea. Rev.,* **105,** 1136–1150.

Franklin, J. L., 1987: Reduction of errors in Omega dropwindsonde data through postprocessing. NOAA Tech. Memo. ERL AOML-54, 22 pp. [Available from NOAA/AOML/HRD, 4301 Rickenbacker Causeway, Miami, FL 33149.]

——, and P. R. Julian, 1985: An investigation of Omega windfinding accuracy. *J. Atmos. Oceanic Technol.,* **2,** 212–231.

Gamache, J. F., and R. A. Houze Jr., 1982: Mesoscale air motions associated with a tropical squall line. *Mon. Wea. Rev.,* **110,** 118–135.

Gentry, R. C., 1983: Genesis of tornadoes associated with hurricanes. *Mon. Wea. Rev.,* **111,** 1793–1805.

Govind, P. K., 1975: Omega windfinding systems. *J. Appl. Meteor.,* **14,** 1503–1511.

Griffith, J. M., 1993: A comparison of the properties and surface fluxes associated with the inflow and downdraft air of tropical MCSs. Preprints, *20th Conf. on Hurricanes and Tropical Meteorology,* San Antonio, TX, Amer. Meteor. Soc., 209–212.

Hawkins, H. F., and S. M. Imbembo, 1976: The structure of a small, intense hurricane, Inez 1966. *Mon. Wea. Rev.,* **104,** 418–442.

Hill, E. L., W. Malkin, and W. A. Schulz Jr., 1966: Tornadoes associated with cyclones of tropical origin—Practical features. *J. Appl. Meteor.,* **5,** 745–763.

Houston, S. H., M. D. Powell, and P. P. Dodge, 1997: Surface wind fields in 1996 Hurricanes Bertha and Fran at landfall. Preprints, *22d Conf. on Hurricanes and Tropical Meteorology,* Fort Collins, CO, Amer. Meteor. Soc., 92–93.

Jordan, C. L., 1958: Mean soundings for the West Indies area. *J. Meteor.,* **15,** 91–97.

——, and E. S. Jordan, 1954: On the mean thermal structure of tropical cyclones. *J. Meteor.,* **11,** 440–448.

Jorgensen, D. P., 1984a: Mesoscale and convective-scale characteristics of mature hurricanes. Part I: General observations by research aircraft. *J. Atmos. Sci.,* **41,** 1268–1285.

——, 1984b: Mesoscale and convective-scale characteristics of mature hurricanes. Part II: Inner core structure of Hurricane Allen (1980). *J. Atmos. Sci.,* **41,** 1287–1311.

Lazarus, S. M., and K. K. Droegemeier, 1990: The influence of helicity the stability and morphology of numerically simulated storms. Preprints, *16th Conf. on Severe Local Storms and Conf. on Atmospheric Electricity,* Kananaskis Park, AB, Canada, Amer. Meteor. Soc., 269–274.

LeMone, M. A., G. M. Barnes, E. J. Szoke, and E. J. Zipser, 1984: The tilt of the leading edge of mesoscale tropical convective lines. *Mon. Wea. Rev.,* **112,** 510–519.

Lilly, D. K., 1986: The structure, energetics and propagation of rotating convective storms. Part II: Helicity and storm stabilization. *J. Atmos. Sci.,* **43,** 126–140.

Malkus, J. E., 1952: The slopes of cumulus clouds in relation to external wind shear. *Quart. J. Roy. Meteor. Soc.,* **78,** 530–542.

——, 1958: On the structure of the trade wind moist layer. Papers in Physical Oceanography and Meteorology 13, Massachusetts Institute of Technology–Woods Hole Oceanographic Institution, 13, 47 pp. [Available from Woods Hole Oceanographic Institution, Woods Hole, MA 02543.]

McBride, J. L., and R. Zehr, 1981: Observational analysis of tropical cyclone formation. Part II: Comparison of non-developing versus developing systems. *J. Atmos. Sci.,* **38,** 1132–1151.

McCaul, E. W., Jr., 1991: Buoyancy and shear characteristics within hurricane tornado environments. *Mon. Wea. Rev.,* **119,** 1954–1978.

——, and M. L. Weisman, 1996: Simulations of shallow supercell storms in landfalling hurricane environments. *Mon. Wea. Rev.,* **124,** 408–429.

Molinari, J., P. K. Moore, V. P. Idone, R. W. Henderson, and A. B. Saljoughy, 1994: Cloud-to-ground lightning in Hurricane Andrew. *J. Geophys. Res.,* **99,** 16 665–16 676.

——, ——, and ——, 1999: Convective structure of hurricanes as revealed by lightning locations. *Mon. Wea. Rev.,* **127,** 520–534.

Moncrieff, M. W., and M. J. Miller, 1976: The dynamics and simulation of tropical cumulonimbus squall lines. *Quart. J. Roy. Meteor. Soc.,* **102,** 373–394.

NCAR, 1977: U.S. GATE central program workshop report. National Center for Atmospheric Research, Boulder, CO, 723 pp.

Newton, C. W., 1966: Circulations in large sheared cumulonimbus. *Tellus,* **18,** 699–713.

Novlan, D. J., and W. M. Gray, 1974: Hurricane spawned tornadoes. *Mon. Wea. Rev.,* **102,** 476–488.

Orton, R., 1970: Tornadoes associated with Hurricane Beulah on September 19–23, 1967. *Mon. Wea. Rev.,* **98,** 541–547.

Pearson, A. D., and A. F. Sadowski, 1965: Hurricane-induced tornadoes and their distribution. *Mon. Wea. Rev.,* **93,** 461–464.

Powell, M. D., 1980: Evaluations of diagnostic marine boundary layer models applied to hurricanes. *Mon. Wea. Rev.,* **108,** 757–766.

——, 1990a: Boundary layer structure and dynamics in outer hurricane rainbands. Part I: Mesoscale rainfall and kinematic structure. *Mon. Wea. Rev.,* **118,** 891–917.

——, 1990b: Boundary layer structure and dynamics in outer hurricane rainbands. Part II: Downdraft modification and mixed layer recovery. *Mon. Wea. Rev.,* **118,** 918–938.

——, and S. H. Houston, 1996: Hurricane Andrew's landfall in south Florida. Part II: Surface wind fields and potential real-time applications. *Wea. Forecasting,* **11,** 329–349.

——, ——, P. Dodge, C. Samsury, and P. G. Black, 1998: Surface wind fields of 1995 Hurricanes Erin, Opal, Luis, Marilyn, and Roxanne at landfall. *Mon. Wea. Rev.,* **126,** 1259–1273.

Rotunno, R., and K. A. Emanuel, 1987: An air–sea interaction theory

for tropical cyclones. Part II: Evolutionary study using a nonhydrostatic axisymmetric numerical model. *J. Atmos. Sci.,* **44,** 542–561.

Sheets, R. C., 1969: Some mean hurricane soundings. *J. Appl. Meteor.,* **8,** 134–146.

Spratt, S. M., D. W. Sharp, P. Welsh, A. Sandrik, F. Alsheimer, and C. Paxton, 1997: A WSR-88D assessment of tropical cyclone outer rainband tornadoes. *Wea. Forecasting,* **12,** 479–501.

Weisman, M. L., and J. B. Klemp, 1982: The dependence of numerically simulated convective storms on vertical wind shear and buoyancy. *Mon. Wea. Rev.,* **110,** 504–520.

——, and ——, 1984: The structure and classification of numerically simulated convective storms in directionally varying wind shears. *Mon. Wea. Rev.,* **112,** 2479–2498.

Williams, E., and N. Renno, 1993: An analysis of the conditional instability of the tropical atmosphere. *Mon. Wea. Rev.,* **121,** 21–36.

Wu, W.-S., D. K. Lilly, and R. M. Kerr, 1992: Helicity and thermal convection with shear. *J. Atmos. Sci.,* **49,** 1800–1809.

Zipser, E. J., 1977: Mesoscale and convective-scale downdrafts as distinct components of squall-line circulation. *Mon. Wea. Rev.,* **105,** 1568–1589.

——, and M. A. LeMone, 1980: Cumulonimbus vertical velocity events in GATE. Part II: Synthesis and model core structure. *J. Atmos. Sci.,* **37,** 2458–2469.